Water Research 245 (2023) 120660

Contents lists available at ScienceDirect

Water Research

journal homepage: www.elsevier.com/locate/watres

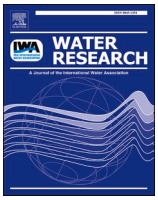

Monitoring settling of anaerobic digestates using low-field MRI profiling and NMR relaxometry measurements

Emanuel G. Bertizzolo [a,b], Charlie G. Gomes [c], Nicholas Ling [a], Fabiana Tessele [b], Michael L. Johns [a], Einar O. Fridjonsson [a,*]

[a] Department of Chemical Engineering, The University of Western Australia, 6009, Australia
[b] Tessele Consultants, 6156, Australia
[c] Chemical Metrology Laboratory, Federal University of Pelotas, 96010-900, Brazil

ARTICLE INFO

Keywords:
Anaerobic digestate
Flocculation
Settling process
Water removal
NMR & MRI

ABSTRACT

Dewatering of anaerobic digestate from red meat processing was assessed using low field MRI profiling and NMR relaxometry. Samples were flocculated using a cationic flocculant (EM640CT) at dosing range (0 to 1.6% v/v) and monitored during the initial 30 min of settling via MRI profiling to assess changes in water fraction, settling time and initial settling velocity. The profiles showed decreasing settling time and increasing initial settling velocity with increased dosing, while sample porosity was observed to increase up to the optimal dosing point (0.8% v/v). Significant increases in sample variability were observed past this point due to flocculant overdosing. The samples were then analysed in terms of turbidity and NMR relaxometry. Increasing flocculant concentration caused turbidity to decrease from 210 to 13 NTU. The relaxation rate of free water showed a strong positive correlation with turbidity. T_2 peaks observed before overdosing could be assigned to different water structures (free, interstitial, vicinal and hydration). An additional T_2 population emerged in the T_2 distributions at the optimal dosing point. Multivariate exploratory data analysis (MEDA) showed that this T_2 population from the solids layer was strongly correlated with the total solids layer height and turbidity of the watery layer. This T_2 peak formation may therefore be used to study opaque flocculated solids to monitor for water structures associated with flocculant overdosing. Further studies using this technique will aim to assess the potential of low field T_2 relaxometry monitoring inline before mechanical dewatering, to monitor optimal flocculant dosing during continuous operations on systems with high solids concentration.

1. Introduction

With global awareness increasing of the risks associated with non-sustainable strategies, an increasing focus has been placed on circular economy solutions for both long-term environmental and economic sustainability. However, overcoming current linear economy drivers is challenging (Ellen-MacArthur-Foundation, 2015; Schröder and Raes, 2021; Tessele-Consultants, 2022; Ware and Power, 2016). A strategy to reach this circularity is by using bio-wastes (e.g. municipal and agricultural) as a source for anaerobic digestion (Antille et al., 2018; Chojnacka et al., 2020; Lukehurst et al., 2010; Ramirez et al., 2021). The biogas produced by anaerobic digestion can be used in Combined Heat and Power (CHP) engines (Lantz, 2012; Nazari et al., 2021) while the anaerobic digestate which is rich in nitrogen and phosphorous may be further processed into biofertilisers (Drosg et al., 2015; Monfet et al., 2018; Vaneeckhaute et al., 2017).

Dewatering of anaerobic digestate is an important step in fertilizer production due to both the reduction in material volume for transportation and the lowering of water content to reduce heating-power requirements of further biochar conversion (Gopinath et al., 2021; Li et al., 2020) and torrefaction (Doddapaneni et al., 2018; Isemin et al., 2019; Lin et al., 2022) of the solid phase. To achieve sufficient dewatering, flocculation is commonly used prior to mechanical separation (Hyrycz et al., 2022). In practice, wastewater treatment plant operators typically use visual analysis and turbidity measurements to assess the flocculation process. Joannis et al. in 2008, systematically studied the reproducibility and uncertainty of wastewater turbidity measurements, and demonstrated aspects ranging from operator variability, wavelength and measurement principle as sources of significant uncertainties. Because of this, more robust and reliable techniques such as

* Corresponding author.
E-mail address: einar.fridjonsson@uwa.edu.au (E.O. Fridjonsson).

https://doi.org/10.1016/j.watres.2023.120660
Received 24 May 2023; Received in revised form 13 August 2023; Accepted 21 September 2023
Available online 21 September 2023

zeta-potential analysis, are commonly used to complement turbidity analysis (Morfesis et al., 2009). These techniques however can be compromised in samples which contain high particle concentrations and density differences, requiring sample dilution. In cases where the focus is on solid waste handling and to quantify the efficiency of such processes, it is important to also assess the solids settling and solids layer properties (Asensi et al., 2019; Babak et al., 2021). Parameters such as turbidity, porosity, settling time and initial settling velocity, are important when optimizing flocculation and mechanical separation steps since they provide information about homogeneity, watery layer clarification, relative amount of solids as feed for selected dewatering equipment and how fast flocs are separating from the watery layer.

To study the settling behavior of solids in suspensions a range of techniques are commonly used such as physical separation (Skinner et al., 2015; Subramanian et al., 2010), optical (Long and Dabros, 2005; Orwin and Smart, 2005), acoustic (Dong et al., 2022; Thorne et al., 2014) and electrical techniques (López-Maldonado et al., 2014; Romero et al., 2018), X-ray tomography (Hu et al., 2020) and nuclear magnetic resonance (NMR) (Beyea et al., 2003; Duval et al., 2010). In this work we study settling using low magnetic field (LF) NMR relying on bulk fluid measurements, therefore circumventing optical issues such as sampling window fouling. An advantage of NMR is that it allows the simultaneous tracking of water fraction in both the settling layer and the bulk solids layer (Mao et al., 2016; Rao et al., 2019; Zhang et al., 2023). LF NMR relaxometry has previously been used to monitor the pore structure of municipal sludge cakes after ultra high-pressure mechanical compaction (Rao et al., 2019), and to assess the applicability and accuracy of LF NMR for the measurement of wastewater water content (Zhang et al., 2023). Here we monitor the flocculant aided settling of anaerobic digestate samples at different flocculant concentrations using T_2 relaxation and 1D magnetic resonance imaging (MRI) and compare the results with traditional turbidity monitoring (Acosta-Cabronero and Hall, 2009; Cabrera et al., 2009). The aim here is to demonstrate the capabilities of the low-field MRI and NMR relaxometry monitoring to quantitatively track the change in solids layer composition during settling to evaluate the effectiveness of dewatering using a commercial flocculant. To highlight the complementary benefits of turbidity and NMR measurements, multivariate exploratory data analysis (MEDA) was applied to quantify the correlation between measured parameters in the study.

2. Materials and methods

2.1. Flocculant treatment and turbidity analysis

To investigate the dewatering process, anaerobic digestate was collected from an anaerobic pond of a red meat processing plant in WA, Australia. The samples were flocculated using an adapted version of the ASTM D2035–19 procedure to find the optimal dosing by conducting jar tests and measuring the top layer turbidity using a Thermo Scientific Eutech TN-100 turbidimeter. 1 L of sample was added to a 1 L glass beaker and mixed using a paddle mechanical stirrer at 300 rpm. A range of 0 to 1.6% v/v (in increments of 0.2% v/v) of flocculant EM640CT by SNF Australia, containing 0.41% wt of active component, was added and mixed for one minute. At each flocculant concentration the mixing speed was then reduced to 60 rpm for one minute to promote flocculation. 10 mL of the watery layer at each increment was sampled and inserted into the Thermo Scientific Eutech TN-100 turbidimeter for turbidity measurements. Subsequently, three samples at each of the nine flocculant concentrations were prepared in 50 mL glass bottles to produce twenty-seven samples to be analyzed using NMR.

2.2. Nuclear magnetic resonance experiments

2.2.1. 1D MRI

Samples in triplicate were measured using a standard 1D MRI pulse sequence ('Profile Scanner') from Oxford GeoSpec 12.7 MHz (Oxford Instruments), one scan was performed every 10 s for 30 min to produce 180 1D signal profiles, using echo time (t_E) of 8 ms, read gradient (G_{read}) of 0.13T/m with 512 acquisition points. Deionized water samples in triplicate were used at the start and end of each set of measurements, as a reference for water content calculations and to detect sample holder location shifts. An in-house MATLAB (R2021a) code was used to perform data analysis and to combine the 180 1D signal profiles to produce signal maps (see Fig. 1). These signal maps were then used to quantify settling time ($t_{settling}$) by tracking the solids/liquid interface (Water content = 0.85 ± 0.01, indicated on Fig. 1 by the blue line) across each map and quantifying the time (t) taken for this interface to reach within 1 mm of the height at t = 30 min, with the subsequent gradual sample height change due to solids compaction. The 1 mm dimension is empirical, and allows better comparison with traditional optically deduced settling time, as the roughness of the surface interface made visual assessment of settling time difficult at finer length-scales. The initial settling velocity (ISV) was calculated using the time (t) taken to reach half the total height change.

2.2.2. T_2 relaxometry

T_2 CPMG experiments were performed at the conclusion of acquiring the 30 min duration 1D MRI signal map for each sample. Four scans of 25,000 echoes were acquired with an echo time of 300 μs. The acquired signal was regularized to obtain T_2 relaxation time distributions as per previously published work (Bristow et al., 2021; Nasharuddin et al., 2021). To assess the signal contribution from different T_2 signal peaks, the resultant T_2 distributions were then fit using a multi-peak Gaussian curve fitting procedure as per S1 in supplementary material. This procedure allows for the mean T_2 and signal contribution from each peak to be quantified. Fig. 2 shows an example of the fitting of a T_2 distribution and the resultant mean T_2 and signal fraction for each peak (calculated by area – see supplementary material). Peak numbering convention is based on its location, starting at P1 for the longest T_2 peak, with peak number increasing with decreasing T_2 value as represented in Fig. 2.

2.3. Multivariate exploratory data analysis (MEDA)

All statistical analyses were performed using Statistica 7.0 software (Statsoft., 2004) and Microsoft Excel software (Microsoft, 2021). Principal component analysis was performed, considering correlations between the quantification of each variable obtained (Vicini et al., 2020). The measurement parameters assessed using the MEDA were the (i) solids height (visual and MRI), (ii) turbidity, (iii) settling time, (iv) initial settling velocity, (v) mean T_2 and (vi) signal fraction for each

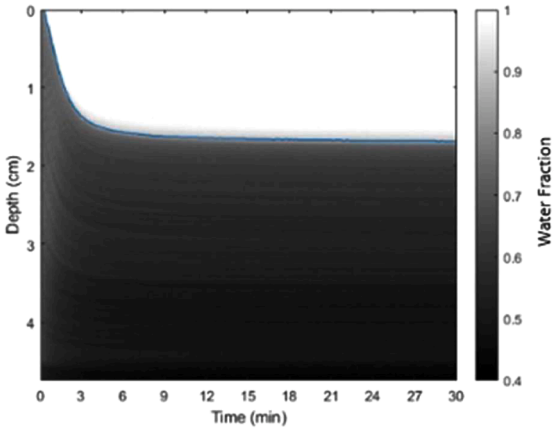

Fig. 1. NMR signal map with depth (cm) from the water-air interface plotted against time (min) for a sample containing no flocculant. The signal map is the combination of 180 1D image profiles acquired every 10 s. The scale bar shows the measured water fraction.

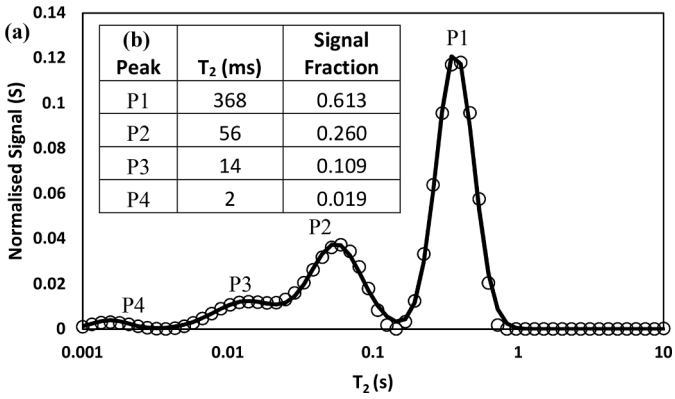

(b) Peak	T_2 (ms)	Signal Fraction
P1	368	0.613
P2	56	0.260
P3	14	0.109
P4	2	0.019

Fig. 2. (a) A T_2 distribution (open circles) and the multi-Gaussian fit to the data (solid line). (b) The results of this fitting tabulated. The signal is normalised such that $\sum S(T_2) = 1$.

distribution peak.

3. Results and discussion

3.1. Turbidity

Fig. 3**a** shows the average turbidity (NTU) of the sampled watery layer as function of flocculant dosing. A decrease in turbidity is observed for flocculant dosing from 0 to 0.6% v/v, with the average turbidity decreasing from 210 to 117 NTU. At 0.8% v/v there is a sharp drop in turbidity to 56 NTU, with a significant reduction in standard deviation from 47.4 NTU to 3.5 NTU. From this dosing onwards, there is a more gradual decrease in turbidity reaching an average value of 13 NTU at 1.6% v/v. For reference the inset picture (see Fig. 3**a**) which shows photographs of samples containing 0, 0.8 and 1.6% v/v of EM640CT, indicating that the watery layer is clarifying with increasing flocculant concentration, while simultaneously, there is an increase in flocculated layer thickness (see Fig. 3**b**).

Polymeric flocculation can separate water from solids in a suspension by neutralization of particle surficial charges, adsorption via attraction of opposite charges and polymer bridging (Hjorth and Jørgensen, 2012). The flocculated solids then arrive homogeneous at the subsequent mechanical separation step, reducing uncertainty in separation performance. The optimal flocculant dosing in the current study is assessed as 0.8% v/v due to the ~73% reduction in turbidity (NTU) and sharp reduction in standard deviation. After measuring turbidity, the total and solids layer heights were measured and the normalised solids height was obtained (see Fig. 3**b**), this shows that as the turbidity decreases there is a corresponding increase in the solid height level of 16% as floc formation causes a reduction in the watery layer due to the formation of thicker layer of flocculated solids. In addition to that, it is noticeable that the solids height profile does not increase as much after the addition of 0.8% v/v of flocculant as before this concentration. This is indicative of the smaller and lighter particles in suspension settling, occupying less volume and filling vacant space, keeping the solids height fairly constant with increasing flocculant dosing. Although the turbidity measurement approach used on the samples is both rapid and low cost, it is intrinsically dependent on light scattering, as such it can provide very limited information about the solids layer. By contrast NMR is capable of monitoring and quantifying this opaque layer. This allows the water fraction across the depth of the sample to be monitored during the settling process allowing the effect of flocculant on each sample's solids structure to be probed. To this end, 1D MRI profiling and T_2 relaxometry measurements were performed respectively during the flocculation/settling and at the conclusion of settling process.

3.2. 1D MRI profiles

Fig. 4**a** shows a selected set of data for 0%, 0.8% and 1.6% v/v (the full sets of 27 signal maps obtained can be found in **S2** of the supplementary material section). Fig. 4**a (a-c)** shows the settling profiles over 30 min for samples with no flocculant added. These show that there is good clarification of solids from the top layer of the samples with sample variability observed. Even after 30 min of settling there is still slow compression settling occurring (Tchobanoglous et al., 2003). This behavior is expected for non-flocculated samples due to its surface charges preventing further solid aggregation, delaying these particles reaching an equilibrium distribution. Fig. 4**b** shows representative profiles at $t = 0$ (t_0) and $t = 30$ min (t_f) obtained from three signal maps at respectively 0, 0.8 and 1.6% v/v flocculant dosing. These emphasize the water fraction profile transitions (seen in Fig. 4**a**) along the depth of the sample with increasing flocculant dosing, with the maximum dosing (1.6% v/v) producing a higher water content (higher porosity) solids layer with a near constant porosity across the depth of the solids layer.

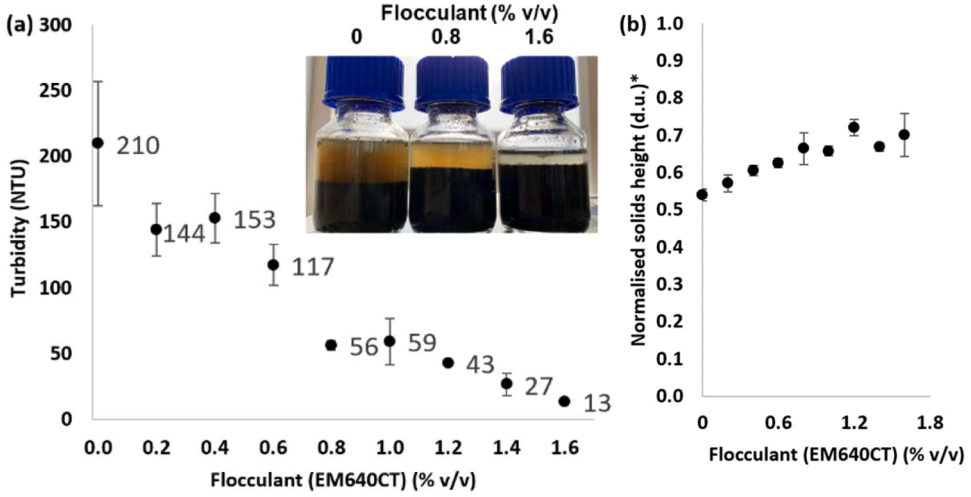

Fig. 3. (a) Measured turbidity (NTU) after 30 min of settling using a turbidity meter versus flocculant concentration (% v/v). Error bars show the standard deviation of measurements performed in triplicate. Inset photograph shows the visual flocculation of 0, 0.8 and 1.6% v/v after 30 min of flocculation. (b) Normalised solid layer height based on visual measurements using a digital caliper after 30 min of settling.
*dimensionless unit.

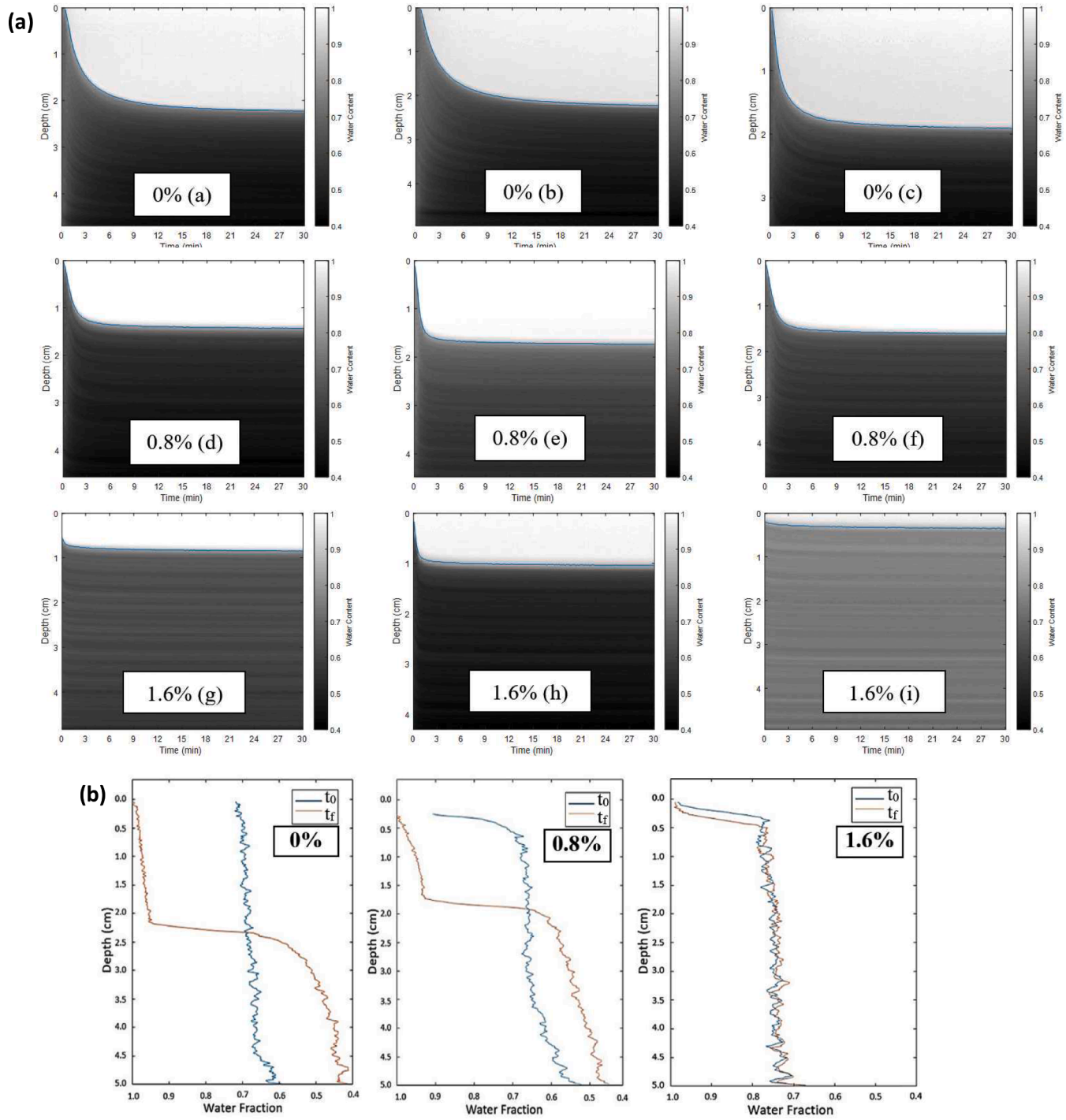

Fig. 4. **(a)** Shows 1D MRI profiles using low-field NMR system plotted with time for three selected samples (0%, 0.8% and 1.6%wt flocculant). The color bar shows equivalent water fraction (from 0.4 to 1) and the blue line tracks water fraction = 0.85±0.01. (b**)** shows water fraction vs. depth profiles at t = 0 min (t_0) and t = 30 min (t_f), these are shown here to show common profile trends with increasing flocculant addition from 0% to 1.6%. As well as to more clearly show the fluctuations in water fraction observed along the depth of the sample.

By contrast the final profiles (t_f) for the 0% and 0.8% v/v show a porosity gradient with lowest water content at the bottom of the container. Another interesting feature of the 1D MRI profiles is the gradient observed in the water layer (0.8% v/v) at t_0 where there is more clarification towards the top of the watery layer than towards the bottom. This is in contrast to the 0% v/v sample where the watery layer has a near constant water content. For the same samples the watery layer at t_f are observed to have similar average water content but very different depths and profile shapes. The richness of the individual water fraction profiles is highlighted in Fig. 4b, with features such as the water content striations seen in Fig. 4a indicating solids stratification during settling.

Fig. 5 shows $t_{settling}$ and initial settling velocity (ISV) where in comparison to the non-flocculated sample, the 0.8% v/v and 1.6% v/v samples show a significant reduction in $t_{settling}$ and increase in ISV, however these samples have on average a much thinner watery layer. In the case of 0.8% v/v of flocculant, the formation of dense flocs promotes quicker separation quantified by a 65% reduction in $t_{settling}$ and an 81% increase in initial settling velocity. When the dosing rises to 1.6% v/v,

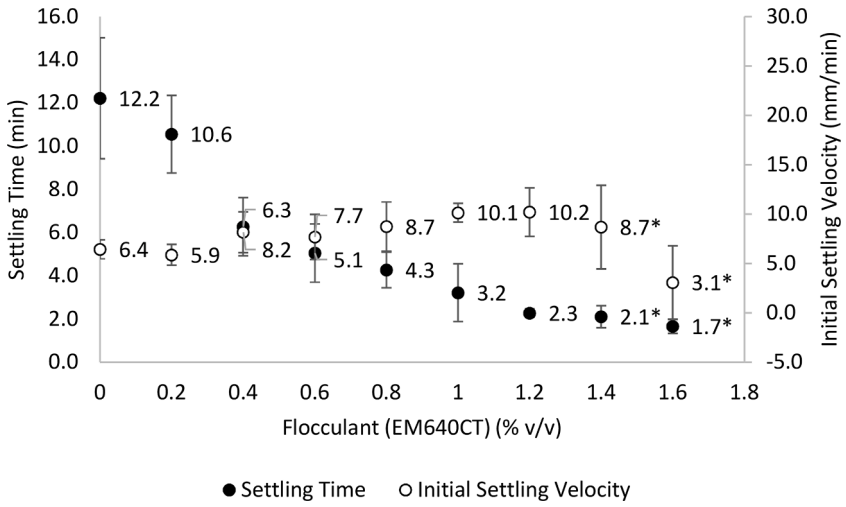

Fig. 5. Shows average settling time (min) and average initial settling velocity (mm/min) versus flocculant concentration (% v/v).
*(Initial Settling Velocity could not be accurately assessed due to rapid settling (<10 s) at the highest flocculant doses (1.4 and 1.6% v/v)).

the 1D MRI profiles show increasing variability across the triplicate samples which has been previously observed due to flocculant overdosing (Hjorth and Jørgensen, 2012). This is contrasted by turbidity which shows the smallest standard deviation and lowest value of turbidity (see Fig. 5). When assessed visually, the overdosed systems with 1.4% and 1.6% v/v occur with initial flocculant settling faster than 10 s (see Fig. 4**a(g)** and 4**a(i)**). Due to this, the corresponding calculated $t_{settling}$ and initial settling velocity are labelled with an asterisk in Fig. 5. A trend of decreasing settling time and increasing initial settling velocity up to the last two flocculant concentrations is consistent with expectation that the flocculant induces more rapid settling.

Fig. 6 shows a comparison between the normalized solids height, which was visually assessed, and the water/solids interface height from the 1D MRI profile data. As expected, the results are similar, with the largest deviation in results observed at the greatest solids layer heights where the uncertainty in the measured water layer is the largest for the visual technique due to the loosely flocculated solids layer and due to the visual inspection occurring after the conclusion of the triplicate sample measurements, and therefore affected by slow sample compaction at $t > 30$ min. The error bars show the standard deviation for the triplicate measurements.

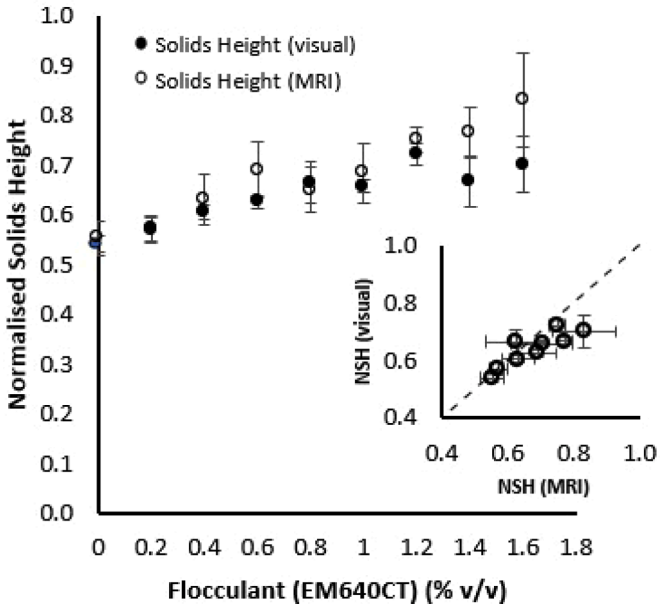

Fig. 6. Shows comparison between normalised solids height measured visually and using 1D MRI profiles. A trend of the solid's height increasing with the addition of flocculant is captured by the MRI but is not as clear visually, which can be explained by the intrinsic error of visually measuring a cloudy solid-liquid interface. Inset figure shows the normalised solids height (NSH) for visual and MRI technique, confirming the deviation at the higher NSH, which corresponds to the higher flocculant dosed samples.

3.3. T_2 relaxation measurements

The T_2 distribution of each sample is shown in Fig. 7**a**. As suspended solids in the watery layer cause enhanced relaxation rates ($R_2 = T_2^{-1}$), the average of the smallest R_2 (which corresponds to the greatest T_2, peak P1 in Fig. 7**a**) was plotted against turbidity (see Fig. 7**b**). Both the R_2 and turbidity decrease with increasing flocculant concentration from 0 to 1.6% v/v with a Pearson correlation coefficient (PCC) of 0.93 (Edwards, 1976). As T_2 relaxation of pure water is ~ 2 s the relaxation rate (R_2) plateaus at ~ 0.5 s^{-1}. This plateauing is observed to occur for the two highest flocculant concentrations. Fig. 7**c** shows the total signal fraction contribution of the two longest T_2 peaks (closed circles) and the remaining shorter T_2 peaks (open circles). This shows water swapping local T_2 relaxation environments with increasing flocculant addition until 0.8% v/v after which there is minimal change. The signal percentage from the longest T_2 peaks start at 89% for no flocculant and decrease to 70% for the highest flocculant concentration (1.6%wt). This effect is consistent with observed increase in solids layer height and therefore porosity of, on average, 22% (see Fig. 6), with more and more water occupying the shorter T_2 peak populations (increasing from 11% to 30%). This is indicative of more of the NMR signal originating from water molecules interacting with solids, with the free water in the system tending to be trapped within flocs caused by increasing polymer concentration.

For flocculated sludge systems it is known that there are four different water structures: Free, Interstitial, Vicinal and Hydration water (Vesilind, 1994), see Fig. 8 for a schematic representation. Given that lower T_2 relaxation water populations should correspond with proximity to solids, the order of the peaks from longest to shortest T_2, on sample containing 0% to 0.6% v/v for example, in Fig. 7**a** corresponds well with these four water structures (Free, Interstitial, Vicinal and Hydration water, from longer to shorter T_2 peaks respectively). To validate this interpretation for the current system sample drying (Salamat et al., 2022) was performed which demonstrated that the first water population removed was P1 corresponding with the free water, then the interstitial water was removed, and the remaining shortest T_2 NMR

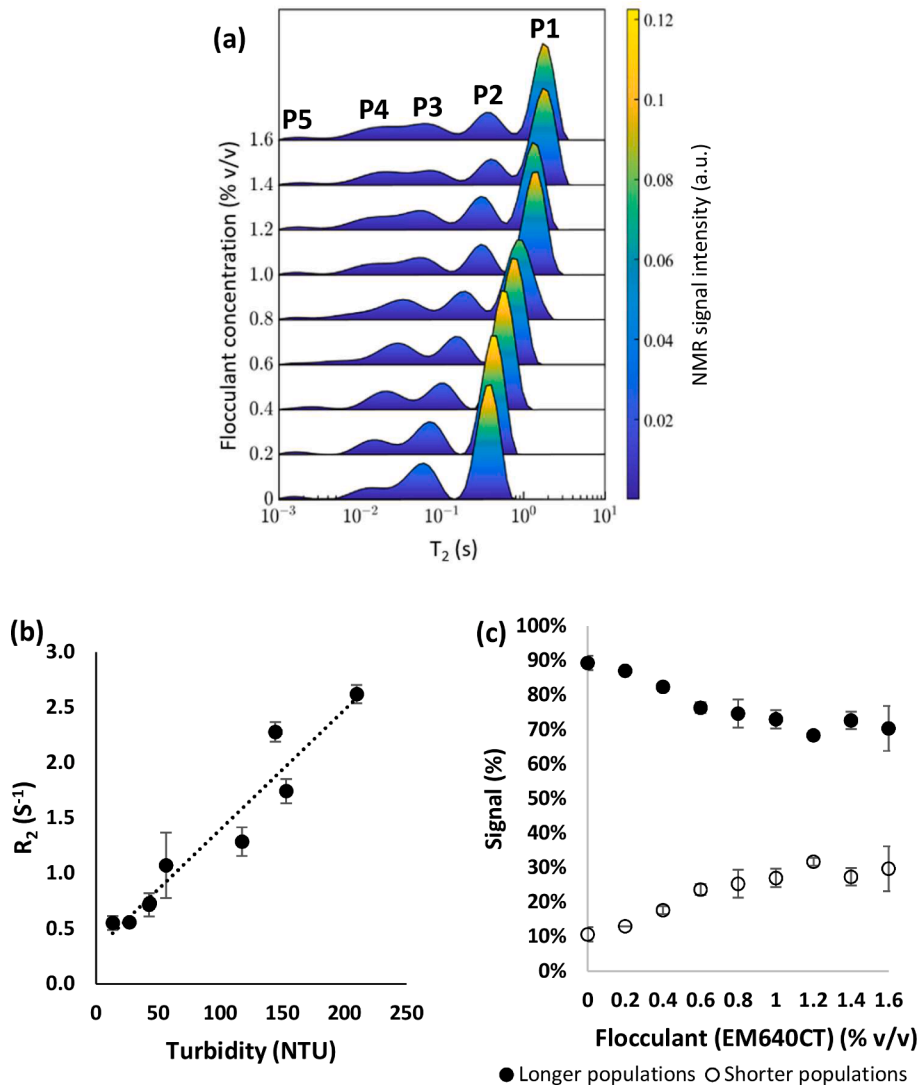

Fig. 7. (a) T_2 distribution of samples versus flocculant concentration. A shift to decreasing relaxation rate (increase in T_2) is observed with increasing flocculant concentration. An additional peak is observed to emerge at >0.6% v/v. (b) shows the correlation of the relaxation rate (R_2) and turbidity for the longest T_2 peak (P1). (c) shows the NMR signal percentage from the longer (P1, P2) and the shorter (P3, P4 and P5) T_2 peaks.

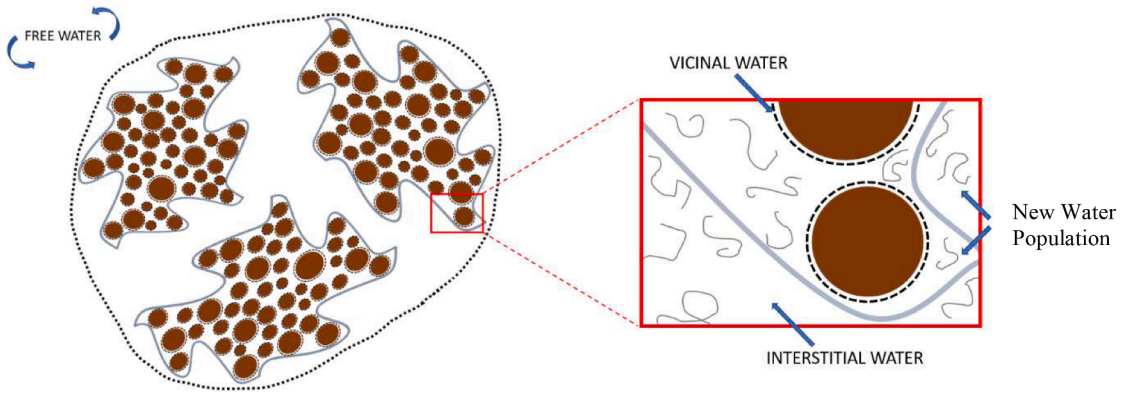

Fig. 8. Diagram shows four postulated water environments. Free water are water molecules away from other materials, Interstitial water are water molecules trapped amongst the different flocs (inside or not), Vicinal water are multiple layers of water molecules at particle surface attracted by intermolecular forces (mainly hydrogen bonding) and the additional water population is water molecules trapped around the extra dosed polymer in the sample. The hydration water, which has the shortest T_2 is not represented in the diagram. Source: Adapted from (Vesilind, 1994).

signal was retained with water molecules associated with the solids (i.e. vicinal and hydration water). An important observation from Fig. 7**a** is that at flocculant concentrations > 0.6% v/v, an additional T_2 peak with mean T_2 ~ 15 ms is observed to emerge and grow as more flocculant is added (refer to **S1**). To represent the effect of polymer addition to the system, the Fig. 8 diagram shows the potential effect of polymer creating a 'fifth' NMR detectable water structure. It is postulated here that this water structure in Fig. 7**a** emerges after the optimal dosing due to flocculant/polymer trapping free water in the flocs and the rearrangement of these flocs. This observation is broadly consistent with results in Fig. 7**c** whereby this new signal peak emerges after the observed reduction in NMR signal contribution from the two longest relaxation populations by 19%. This interpretation is consistent with the flocculant causing the formation of an additional looser/lighter (commonly called "fluffy cake" by operators) structure (Bratby, 2016). The quantitative measurement of this formation by monitoring for an additional T_2 peak is a potentially useful measurement of flocculant overdosing whereby T_2 relaxation measurements can be used to systematically monitor this local structure formation. However, for samples containing high-loading of para- or ferromagnetic species, signal correction techniques may need to be adopted (Carroll et al., 2018), this requires further systematic study beyond the scope of the current research.

To further explore the emergence of the new NMR detected water structure a Multivariate Exploratory Data Analysis (MEDA) was performed. The postulated water populations in Fig. 8 (Free, Interstitial, Vicinal and "New Water Population") are labelled Peak 1, 2, 3 and 4, respectively in the MEDA analysis. The analysis resulted in fourteen principal components, with the two with highest explanation (Factor 1 + Factor 2 = 82%) used to generate the corresponding Cartesian plane plots (see Fig. 9) (Bondu et al., 2020; Filho et al., 2007; Louzada et al., 2022; Vicini et al., 2020). Fig. 9**a** highlights two main opposite groups: $t_{settling}$, R_2 of peak 1 and turbidity on the right-hand side and the two measured solids height on the left-hand side, demonstrating a strong inverse correlation between the groups (e.g. low turbidity in the system corresponds to higher solids height). In Fig. 9**b** T_2 peak values for all four peaks and peak 4 signal fraction (S.F.) are located on the left-hand side implying the longer the T_2 values for all populations, the more relative signal there is from peak 4 (new signal peak measured at flocculant concentration > 0.6% v/v). There is also an inverse relationship with Peak 1 and 2 signal fraction and no significant change of Peak 3 signal fraction. The fact that peak 3 signal fraction does not vary significantly is consistent with expectation if peak 3 corresponds to vicinal water (see Fig. 8) as there is no addition of solids to the system. The MEDA shows that peak 4 is closely related to the solids layer height and T_2 values for all peaks in the sample set, this corresponds with previous observations concerning flocculant overdosing confirming a strong relationship between peak 4 and overdosing, and the effect this has on the T_2 relaxation of the other signal populations in the sample. The MEDA analysis therefore supports the potential usefulness of using the emergence of peak 4 as an indicator for flocculant overdosing.

4. Conclusions

In this work turbidity, 1D MRI profiles and NMR T_2 relaxation measurements were used to monitor the flocculation and settling process of anaerobic digestate from a red meat processing plant. The turbidity analysis showed clarification of the watery layer with the addition of flocculant resulting in a final turbidity value of 13 NTU and solids height up to 70% of total height. Gradual increases in solids height were observed with increasing flocculant concentration both using 1D MRI and visual assessment, whilst faster settling times and initial settling velocity were observed. 1D MRI showed highest sample homogeneity (smallest standard deviation) at the optimal dosing of 0.8% v/v, corresponding to an observed inflexion in turbidity readings when the NTU value was ~27% of the initial NTU value. T_2 measurements showed four initial peaks corresponding to four different water structures (free, interstitial, vicinal and hydration) consistent with flocculated sludge systems (Vesilind, 1994), with a fifth NMR detected water structure emerging after the system experiences flocculant overdosing (>0.6% v/v). Multivariate Exploratory Data Analysis (MEDA) shows that the growth of this new signal peak is strongly positively correlated with T_2 for all peaks and solids height, while strongly negatively correlated with settling time and turbidity. Signal contributions of the longest T_2 peaks (Peak 1 & 2) were shown to negatively correlate with peak 4, while peak 3 showed no correlation. This supports the assessment that peak 3 is vicinal water which doesn't change as the amount of solids doesn't change, rather the addition of flocculant causes water initially occupying peak 1 and 2 (respectively the free and interstitial water structures) to become part of a loose and growing flocculant water structure. These results demonstrate that low field NMR relaxometry is an efficient complementary analysis technique to turbidity measurements by allowing the solids region to be probed, whilst also showing that T_2 relaxation may be used to monitor for signal peak emergence associated with flocculant overdosing. Further studies aim to implement

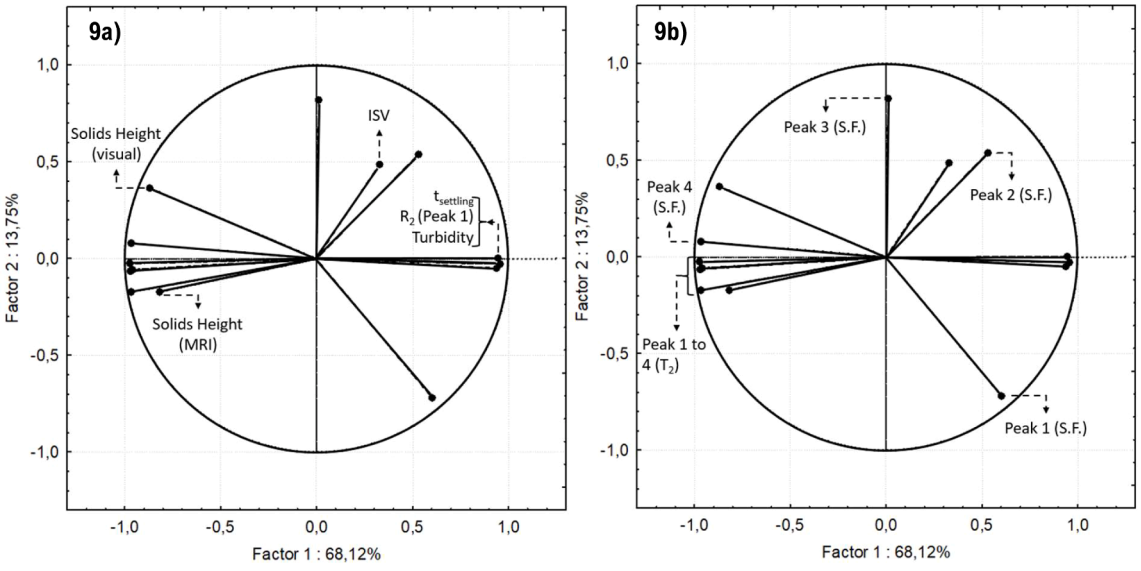

Fig. 9. Shows the Cartesian plane plots resulting from the MEDA analysis. The Euclidean distance between variables in the Cartesian plane allows for the assessment of how strong, positively (near each other) or negatively (radial opposite position) variables are correlated.

this low field T_2 relaxometry inline before mechanical dewatering systems, and to monitor the ability of the monitoring technique to optimize flocculant dosing during continuous operations of high solids concentration systems where optical techniques may provide insufficient information for accurate quantitative assessment of the flocculated state of the system.

Declaration of Competing Interest

The authors declare that they have no known competing financial interests or personal relationships that could have appeared to influence the work reported in this paper.

Data availability

Data will be made available on request.

Acknowledgements

The authors acknowledge funding and material support from the Australian Meat Processor Corporation (AMPC) and V&V Walsh. EB acknowledges UWA Postgraduate Scholarship funding support.

Supplementary materials

Supplementary material associated with this article can be found, in the online version, at doi:10.1016/j.watres.2023.120660.

References

Acosta-Cabronero, J., Hall, L.D., 2009. Measurements by MRI of the settling and packing of solid particles from aqueous suspensions. AlChE J. 55 (6), 1426–1433.
Antille, D.L., McCabe, B.K., Van Der Spek, W., Baillie, C.P., 2018. An investigation into the fertilizer potential of slaughterhouse cattle paunch. Trans. ASABE 61 (1), 87–101.
Asensi, E., Zambrano, D., Alemany, E., Aguado, D., 2019. Effect of the addition of precipitated ferric chloride on the morphology and settling characteristics of activated sludge flocs. Sep. Purif. Technol. 227.
Babak, P., Li, F., Cabrera, S.M., Kantzas, A., 2021. Laboratory monitoring approaches for tailings settling and evaluation of flocculant and coagulant treatments. Can. J. Chem. Eng. 99 (12), 2702–2712.
Beyea, S.D., Altobelli, S.A., Mondy, L.A., 2003. Chemically selective NMR imaging of a 3-component (solid–solid–liquid) sedimenting system. J. Magn. Reson. 161 (2), 198–203.
Bondu, R., Cloutier, V., Rosa, E., Roy, M., 2020. An exploratory data analysis approach for assessing the sources and distribution of naturally occurring contaminants (F, Ba, Mn, As) in groundwater from southern Quebec (Canada). Appl. Geochem. 114, 104500.
Bratby, J., 2016. Coagulation and Flocculation in Water and Wastewater Treatment. IWA Publishing.
Bristow, N.W., Vogt, S.J., Bucs, S.S., Vrouwenvelder, J.S., Johns, M.L., Fridjonsson, E.O., 2021. Novel magnetic resonance measurements of fouling in operating spiral wound reverse osmosis membrane modules. Water Res. 196, 117006.
Cabrera, S.C.M., Bryan, J., Komishke, B., Kantzas, A., 2009. Study of the settling characteristics of tailings using nuclear magnetic resonance technique. Int. J. Min. Reclam. Environ. 23 (1), 33–50.
Carroll, M.R.J., O'Neill, K., Bristow, N.W., Hopper, T., Vogt, S.J., Johns, M.L., Fridjonsson, E.O., 2018. NMR derived water content from high magnetic susceptibility rock cuttings. Miner. Eng. 122, 211–219.
Chojnacka, K., Moustakas, K., Witek-Krowiak, A., 2020. Bio-based fertilizers: a practical approach towards circular economy. Bioresour. Technol. 295, 122223.
Doddapaneni, T.R.K.C., Praveenkumar, R., Tolvanen, H., Rintala, J., Konttinen, J., 2018. Techno-economic evaluation of integrating torrefaction with anaerobic digestion. Appl. Energy 213, 272–284.
Dong, D., Liu, Q., Wang, X., Hu, H., Wu, B., Ren, H., Wang, J., 2022. Regulation of exogenous acyl homoserine lactones on sludge settling performance: monitoring via ultrasonic time-domain reflectometry. Chemosphere 303.
Drosg, B., Fuchs, W., Seadi, T.A., Madsen, M. and Linke, B. 2015 Nutrient Recovery by Biogas Digestate Processing. Bioenergy, I. (ed), IEA Bioenergy.
Duval, F.P., Quellec, S., Trémier, A., Druilhe, C., Mariette, F., 2010. Non-destructive quantification of water gradient in sludge composting with magnetic resonance imaging. Waste Manage. (Oxford) 30 (4), 610–619.
López-Maldonado, E.A., Oropeza-Guzman, M.T., Jurado-Baizaval, J.L., Ochoa-Terán, A., 2014. Coagulation–flocculation mechanisms in wastewater treatment plants through zeta potential measurements. J. Hazard. Mater. 279, 1–10.
Edwards, A.L., 1976. An Introduction to Linear Regression and Correlation. W. H. Freeman.
Ellen-MacArthur-Foundation, 2015. Delivering the Circular Economy: A toolkit for Policymakers. Ellen MacArthur Foundation, p. 176.
Filho, V.R.A., Polito, W.L., Neto, J.A.G., 2007. Comparative studies of the sample decomposition of green and roasted coffee for determination of nutrients and data exploratory analysis. J. Braz. Chem. Soc. 18, 47–53.
Gopinath, A., Divyapriya, G., Srivastava, V., Laiju, A.R., Nidheesh, P.V., Kumar, M.S., 2021. Conversion of sewage sludge into biochar: a potential resource in water and wastewater treatment. Environ. Res. 194, 110656.
Hjorth, M., Jørgensen, B.U., 2012. Polymer flocculation mechanism in animal slurry established by charge neutralization. Water Res. 46 (4), 1045–1051.
Hu, P., Liang, L., Xie, G., Zhou, S., Peng, Y., 2020. Effect of slurry conditioning on flocculant-aided filtration of coal tailings studied by low-field nuclear magnetic resonance and X-ray micro-tomography. Int. J. Min. Sci. Technol. 30 (6), 859–864.
Hyrycz, M., Ochowiak, M., Krupińska, A., Włodarczak, S., Matusza, M., 2022. A review of flocculants as an efficient method for increasing the efficiency of municipal sludge dewatering: mechanisms, performances, influencing factors and perspectives. Sci. Total Environ. 820, 153328.
Isemin, R., Klimova, D., Larinaa, O., Sytcheva, G., Zaichenkoa, V., Milovanov, O., 2019. Application of torrefaction for recycling bio-waste formed during anaerobic digestion. Fuel 243, 230–239.
Lantz, M., 2012. The economic performance of combined heat and power from biogas produced from manure in Sweden - A comparison of different CHP technologies. Appl. Energy 98, 502–511.
Li, C., Li, J., Pan, L., Zhu, X., Xie, S., Yu, G., Wang, Y., Pan, X., Zhu, G., Angelidaki, I., 2020. Treatment of digestate residues for energy recovery and biochar production: from lab to pilot-scale verification. J. Clean. Prod. (265), 121852
Lin, Y.-L., Zheng, N.-Y., Wang, H.-C., 2022. Sludge dewatering through H2O2 lysis and ultrasonication and recycle for energy by torrefaction to achieve zero waste: an environmental and economical friendly technology. Renew. Sustain. Energy Rev. 155, 111857.
Long, Y., Dabros, T., 2005. Monitoring the settling of water-solids-asphaltenes aggregates using in-line probe coupled with a near-infrared spectrophotometer. Energy Fuels 19 (4), 1542–1547.
Louzada, A.R.d.R., Oliz, L.d.O., Gomes, C.G., Bonemann, D.H., Scherdien, S.H., Ribeiro, A.S., Vieira, M.A., 2022. Assessment of total concentration and bioaccessible fraction of minerals in peaches from different cultivars by MIP OES. Food Chem. 391, 133228.
Lukehurst, C.T., Frost, P., Al Seadi, T., 2010. Utilisation of Digestate from Biogas Plants as Biofertiliser. IEA Bioenergy, pp. 1–36.
Mao, H., Wang, F., Mao, F., Chi, Y., Lu, S., Cen, K., 2016. Measurement of water content and moisture distribution in sludge by 1H nuclear magnetic resonance spectroscopy. Dry. Technol. 34 (3), 267–274.
Monfet, E., Aubry, G., Ramirez, A.A., 2018. Nutrient removal and recovery from digestate: a review of the technology. Biofuels 9 (2), 247–262.
Morfesis, A., Jacobson, A.M., Frollini, R., Helgeson, M., Billica, J., Gertig, K.R., 2009. Role of zeta potential in the optimization of water treatment facility operations. Ind. Eng. Chem. Res. 48, 2305–2309.
Nasharuddin, R., Luo, G., Robinson, N., Fourie, A., Johns, M.L., Fridjonsson, E.O., 2021. Understanding the microstructural evolution of hypersaline cemented paste backfill with low-field NMR relaxation. Cem. Concr. Res. 147, 106516.
Nazari, A., Soltani, M., Hosseinpour, M., Alharbi, W., 2021. Integrated anaerobic co-digestion of municipal organic waste to biogas using geothermal and CHP plants: a comprehensive analysis. Renew. Sustain. Energy Rev. 152, 111709.
Orwin, J.F., Smart, C.C., 2005. An inexpensive turbidimeter for monitoring suspended sediment. Geomorphology 68, 3–15.
Ramirez, J., McCabe, B., Jensen, P.D., Speight, R., Harrison, M., van den Berg, L., O'Hara, I., 2021. Wastes to profit: a circular economy approach to value-addition in livestock industries. Anim. Prod. Sci. 61 (6), 541–550.
Rao, B., Su, X., Qiu, S., Xu, P., Lu, X., Wu, M., Zhang, J., Zhang, Y., Dong, W., 2019. Meso-mechanism of mechanical dewatering of municipal sludge based on low-field nuclear magnetic resonance. Water Res. 162, 161–169.
Romero, C.P., Jeldres, R.I., Quezada, G.R., Concha, F., Toledo, P.G., 2018. Zeta potential and viscosity of colloidal silica suspensions: effect of seawater salts, pH, flocculant, and shear rate. Colloids Surf. A 538, 210–218.
Salamat, R., Scaar, H., Weigler, F., Berg, W., Mellmann, J., 2022. Drying of biogas digestate: a review with a focus on available drying techniques, drying kinetics, and gaseous emission behavior. Dry. Technol. 40 (1), 5–29.
Schröder, P., Raes, J., 2021. Financing an Inclusive Circular Economy. De-Risking Investments for Circular Business Models and the SDGs. Environment and Society Programme, Chatham House.
Skinner, S.J., Studer, L.J., Dixon, D.R., Hillis, P., Rees, C.A., Wall, R.C., Cavalida, R.G., Usher, S.P., Stickland, A.D., Scales, P.J., 2015. Quantification of wastewater sludge dewatering. Water Res. 82, 2–13.
Subramanian, S.B., Yan, S., Tyagi, R.D., Surampalli, R.Y., 2010. Extracellular polymeric substances (EPS) producing bacterial strains of municipal wastewater sludge: isolation, molecular identification, EPS characterization and performance for sludge settling and dewatering. Water Res. 44 (7), 2253–2266.
Tchobanoglous, G., Burton, F.L., Stensel, H.D., 2003. Metcalf & Eddy, Inc. Wastewater Engineering: Treatment and Reuse. McGraw-Hill Companies, Inc.
Tessele-Consultants, 2022. V&V Integrated Waste Management: Integrated Wastewater Treatment, Biogas and Biofertiliser FEED. Australian Meat Processor Corporation, p. 70.
Thorne, P.D., MacDonald, I.T., Vincent, C.E., 2014. Modelling acoustic scattering by suspended flocculating sediments. Cont. Shelf Res. 88, 10.

Vaneeckhaute, C., Lebuf, V., Michels, E., Belia, E., Vanrolleghem, P.A., Tack, F.M.G., Meers, E., 2017. Nutrient recovery from digestate: systematic technology review and product classification. Waste Biomass Valorizat. 8, 21–40.
Vesilind, P.A., 1994. The role of water in sludge dewatering. Water Environ. Res. 66 (1), 4–11.
Vicini, L., Souza, A.M., Morales, F.E.C., Souza, F.M., 2020. Técnicas Multivariadas Exploratórias: Teorias e Aplicações No Software Statistica(C). Editora UFSM.
Ware, A., Power, N., 2016. Biogas from cattle slaughterhouse waste: energy recovery towards an energy self-sufficient industry in Ireland. Renew. Energy 97, 541–549.
Zhang, Y.-L., Sun, P., Dai, B.-B., Zheng, S.-M., Ran, D.-D., Wu, T.-X., Zeng, R.J., Wang, H.-F., 2023. What affects the accuracy and applicability of determining wastewater sludge water content via low-field nuclear magnetic resonance? Environ. Res. 226, 115702.